

The Dust Comportment in the Latitudinal Band 10° North - 20° North in Africa: Emission and Deposition

Abdoulaye Bouya Diop¹, Abdoulaye Sy^{1,2}, Abdoul Karim Mbodji¹, Abdou Karim Farota¹, Malick Wade¹, Adoum Mahamat Moussa^{1,3}, Babacar Niang¹, Aichetou Dia Diop¹, Bara Ndiaye¹, Bouya Diop^{1*}, Amadou Thierno Gaye⁴, Aboubakary Diakhaby¹

¹Gaston Berger University of Saint Louis, Saint Louis, Senegal

²University of Clermont Auvergne, Clermont-Ferrand, France

³University of Chad, Ndjamena, Chad

⁴Cheikh Anta Diop University of Dakar, Dakar, Senegal

Email: *bouyadiop@gmail.com

How to cite this paper: Diop, A. B., Sy, A., Mbodji, A. K., Farota, A. K., Wade, M., Moussa, A. M., Niang, B., Diop, A. D., Ndiaye, B., Diop, B., Gaye, A. T., & Diakhaby, A. (2022). The Dust Comportment in the Latitudinal Band 10° North - 20° North in Africa: Emission and Deposition. *Journal of Geoscience and Environment Protection*, 10, 139-159.

<https://doi.org/10.4236/gep.2022.105011>

Received: March 23, 2022

Accepted: May 28, 2022

Published: May 31, 2022

Copyright © 2022 by author(s) and Scientific Research Publishing Inc. This work is licensed under the Creative Commons Attribution International License (CC BY 4.0).

<http://creativecommons.org/licenses/by/4.0/>



Open Access

Abstract

The three measurement periods: the TOMS Nimbus-7 TOMSN7L3 v008 from 1978 to 1993, the TOMS EP TOMSEPL3 v008 from 1996 to 2005 and the OMI OMTO3d v003 from 2004 to 2008 have allowed the presence of dust to be observed in the 10° North to 20° North latitudinal band (10 - 20 band) of Africa. The 10 - 20 band has a permanent dust presence. The AERONET data show AOD peaks exceeding 2 in Senegal and Niger (on an AOD scale). The statistical study reveals intra-annual relationships in deposition. In Senegal, a significant deposition is observed.

Keywords

Dust, Source Area, AOD, 10° North - 20° North African Band, Deposition, Sahel

1. Introduction

The mechanisms of aerosol lifting, transport and deposition are fairly well documented in the literature (Marticorena & Bergametti, 1995). Source zones have been identified, namely the Bodélé depression and many others (Abouchami et al., 2013; Hudson-Edwards et al., 2014; Bouet et al., 2012; Goodman et al., 2019); others will continue to appear with the advance of the desert due to deforestation (Li et al., 2020), not to mention the fact that the Sahel experienced a long drought from 1970 to 1980 followed by a partial recovery of rainfall which

remains deficient until now (Lebel & Vischel, 2005). Correlations between wind, temperature and rainfall during the African monsoon season (Hassane et al., 2016; Touré et al., 2019; Adenira et al., 2019; Huber & Fensholt, 2011; Janicot, 2009) have been established.

The post-passage deposition of UV Index aerosols “AUVI” in the latitudinal band 10°N - 20°N is very important. These aerosols cover all surfaces, especially solar collectors and panels (Memiche et al., 2020), which can have an impact on their performance.

The objective of this work is to study the distribution of UV index aerosols, and the optical depth. The objective of this work is to study the distribution of UV index aerosols, and the optical depth, and to make a climatic and statistical study of the deposition in order to better understand the mechanisms of lifting, transport, and deposition of aerosols in the 10 - 20 band.

2. Study Area and Method

Our study area is the portion of the land belt around latitudes 10° North and 20° North (10 - 20 band) delineated in the African continent. It contains the Sahelian zone one of the largest and most important dust emission regions (Dirk et al., 2013). With atypical climatic features that few other areas on the globe experience. The 10 - 20 band is mainly characterised by the seasonal movement of the inter-tropical convergence zone (ITCZ). There is: a more or less balanced alternation of dry and wet years from 1900 to 1950, a rainy period from 1950 to 1970 since 1970 a strong period of drought (Ali, 2008) (Figure 1) and a dry advection rich in aerosols (Buontempo et al., 2010; Lézine et al., 2011; Lavaysse et al., 2009). All this results in a significant impact both from a health point of view (Apoil & Yacouba, 2018), and from an environmental point of view (Durand & Lang, 1991). Not to mention the considerable impact that the climate of this area has on the rest of the planet (Alimen, 1897).

Data from point observations (Dakar, Banizoumbou) are provided by AERONET

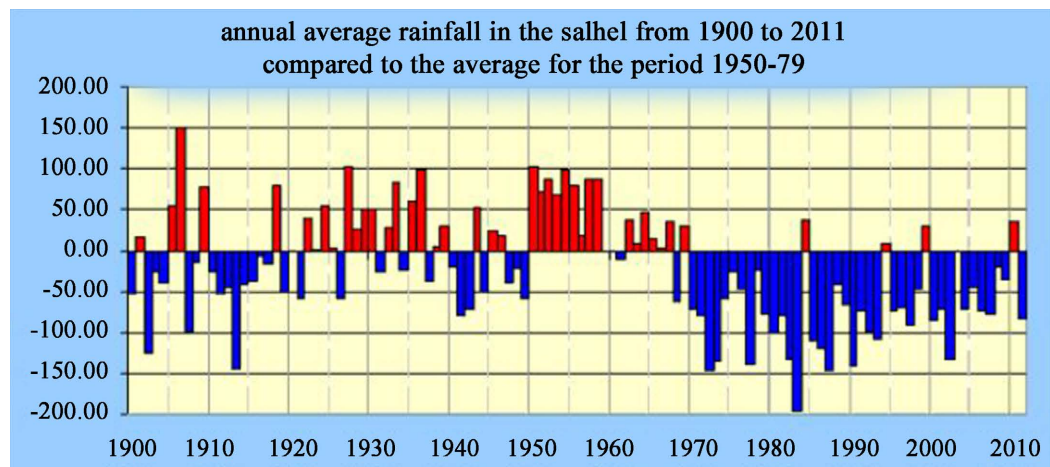


Figure 1. The evolution of the rainfall anomaly in the Sahel from 1900 to 2011 compared to the average from 1950 to 1979. Source JJASO. Image from sècheresse (free.fr).

(Aerosol Robotic Network) which is a ground-based aerosol measurement network established by NASA and PHOTONS (PHotometry for Operational Processing of Satellite Normalization, CNES and CNRS-INSU) and is greatly enriched by other networks (RIMA, AeroSpan, AEROCAN and CARSNET) and collaborators from national agencies, institutes, universities, individual scientists and partners. For more than 25 years, the project has provided a long-term, continuous and easily accessible public domain database on aerosol optical, microphysical and radiative properties for aerosol research and characterisation, validation of satellite retrievals and synergy with other databases. The network requires instrument standardisation, calibration, processing and distribution. The AERONET data used here include optical measurements, providing information on the quantities and properties of aerosols contained in the entire atmospheric column (Rajot et al., 2011). These data are also used in the AMMA project.

UV index aerosols (AUVI) and dust depositions are derived from data from the MODIS sensor on the Terra and Aqua satellites (Acker & Leptoukh, 2007). The AUVI data are initially derived from the Total Ozone Mapping Spectrometer (TOMS) version 8 daily global gridded data product (EP) containing total column ozone, UV aerosol index, Lambertian effective surface reflectivity (Rayleigh corrected) and local noontime UV-B irradiances. The data are considered in a global grid of size $180^\circ \times 288^\circ$ with a lat-long resolution of 1.00×1.25 degrees.

The AUVI are also obtained from the OMI science team. The OMTO3d product is produced by meshing and averaging only good quality orbital data over the total ozone level 2 (OMTO3, based on the improved TOMS version-8 algorithm) on grids of resolutions $1^\circ \times 1^\circ$.

In our work, we will query the three measurement periods TOMS Nimbus-7 TOMSN7L3 v008 from 1978 to 1993, TOMS EP TOMSEPL3 v008 from 1996-2005 and OMI OMTO3d v003 from 2004 to 2008.

These data are pre-processed by Acker in 2014 on the <https://giovanni.gsfc.nasa.gov/giovanni/platform> (Acker, et al., 2014; Hooker & McClain, 2000; Tassan, 1994). Many studies have been carried out on these data, including those commissioned by the AMMA project (Redelsperger et al., 2006) and works such as (Kahn et al., 2005; Basar et al., 2009; Si et al., 2019).

The following parameters: Evaporation, evapotranspiration, geopotential at 1000 hPa, total precipitation, soil type, temperature at 2 meters, wind at 10 meters, vertical velocity, volumetric soil water, vorticity at 1000 hPa, specific humidity are directly extracted from the ERA5 platform.

ERA5 is the fifth generation of ECMWF reanalysis for global climate and weather for the last 4 - 7 decades. Currently, data are available from 1979 onwards. ERA5 replaces the ERA-Interim reanalysis (Olauson, 2018; Wang et al., 2019). The data were regridded to a regular lat-lon grid of 0.25 degrees for the reanalysis and 0.5 degrees for the uncertainty estimation. There are four main subsets: hourly and monthly products, both on pressure levels (upper air fields) and single levels (atmospheric, ocean wave and land surface quantities).

3. Results and Discussions

An overview of the UV Index aerosols in the 10 - 20 band is shown in **Figure 2** and **Figure 3**, which show the distribution of AUVI, which includes “desert dust,

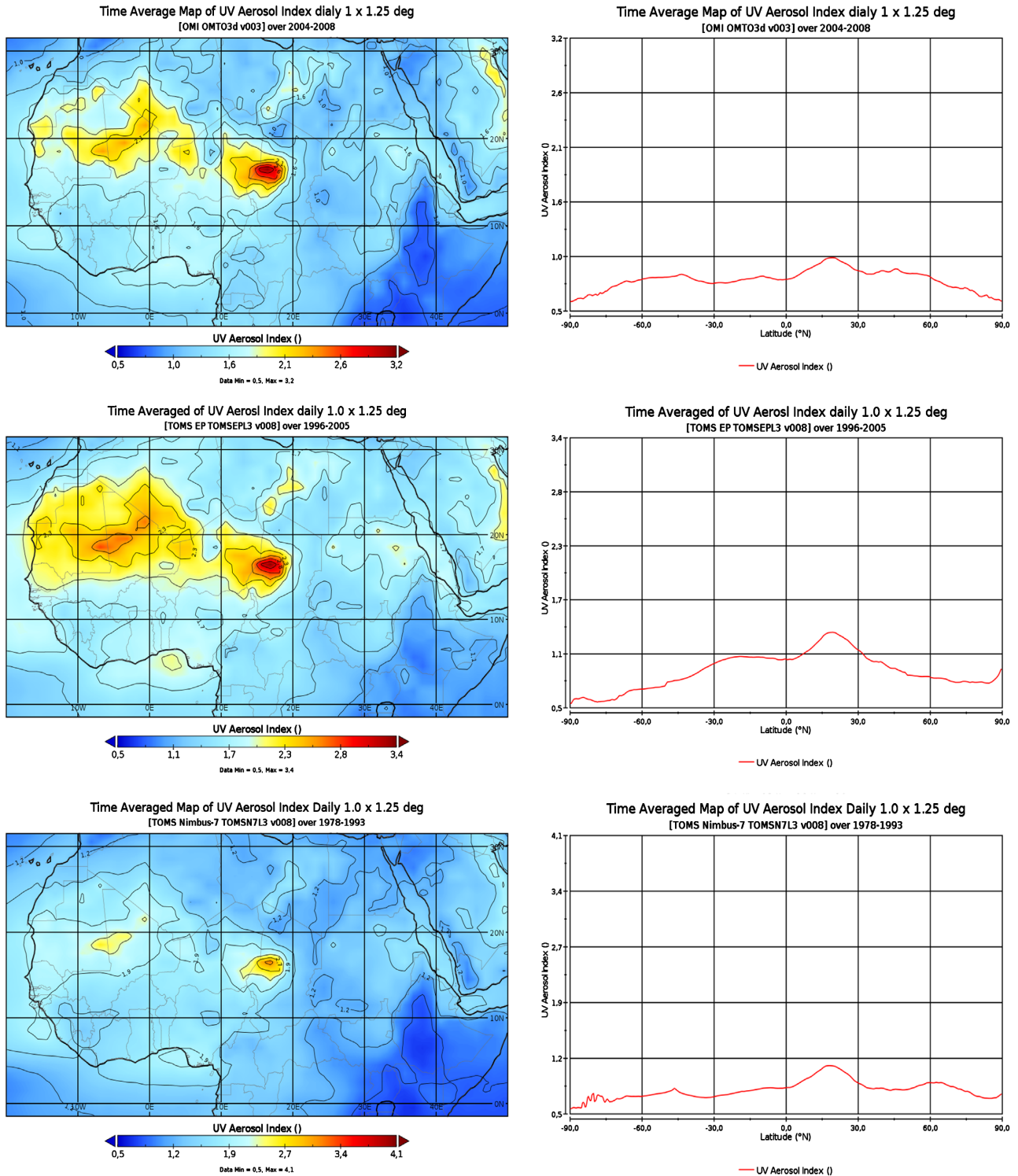
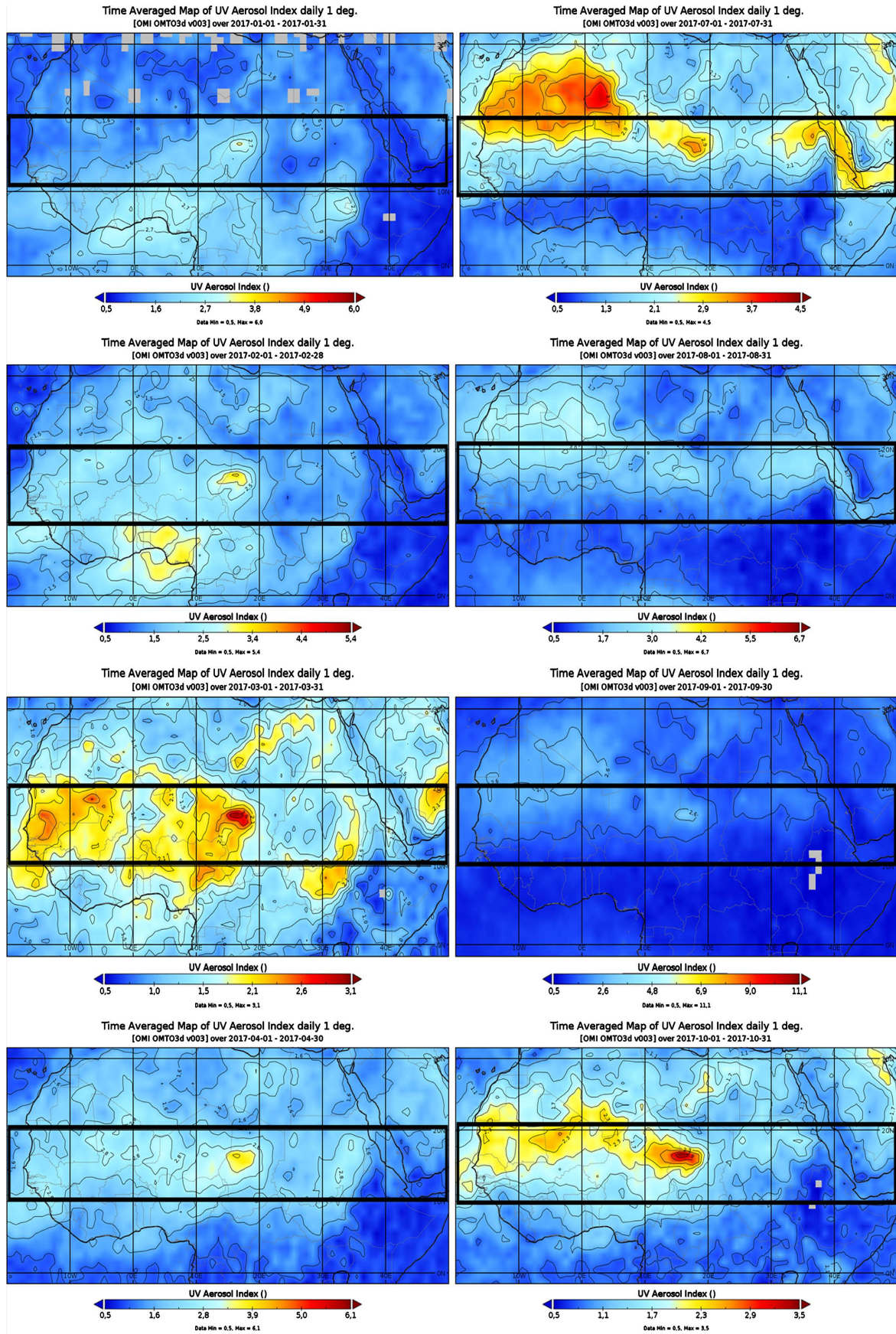


Figure 2. General observation of UV index aerosols during the three measurement campaigns with the OMI 1978-1993 TOMS 1996-2005/2004-2008. Daily average data with a resolution of 1.0×1.25 (from the Giovanni platform).



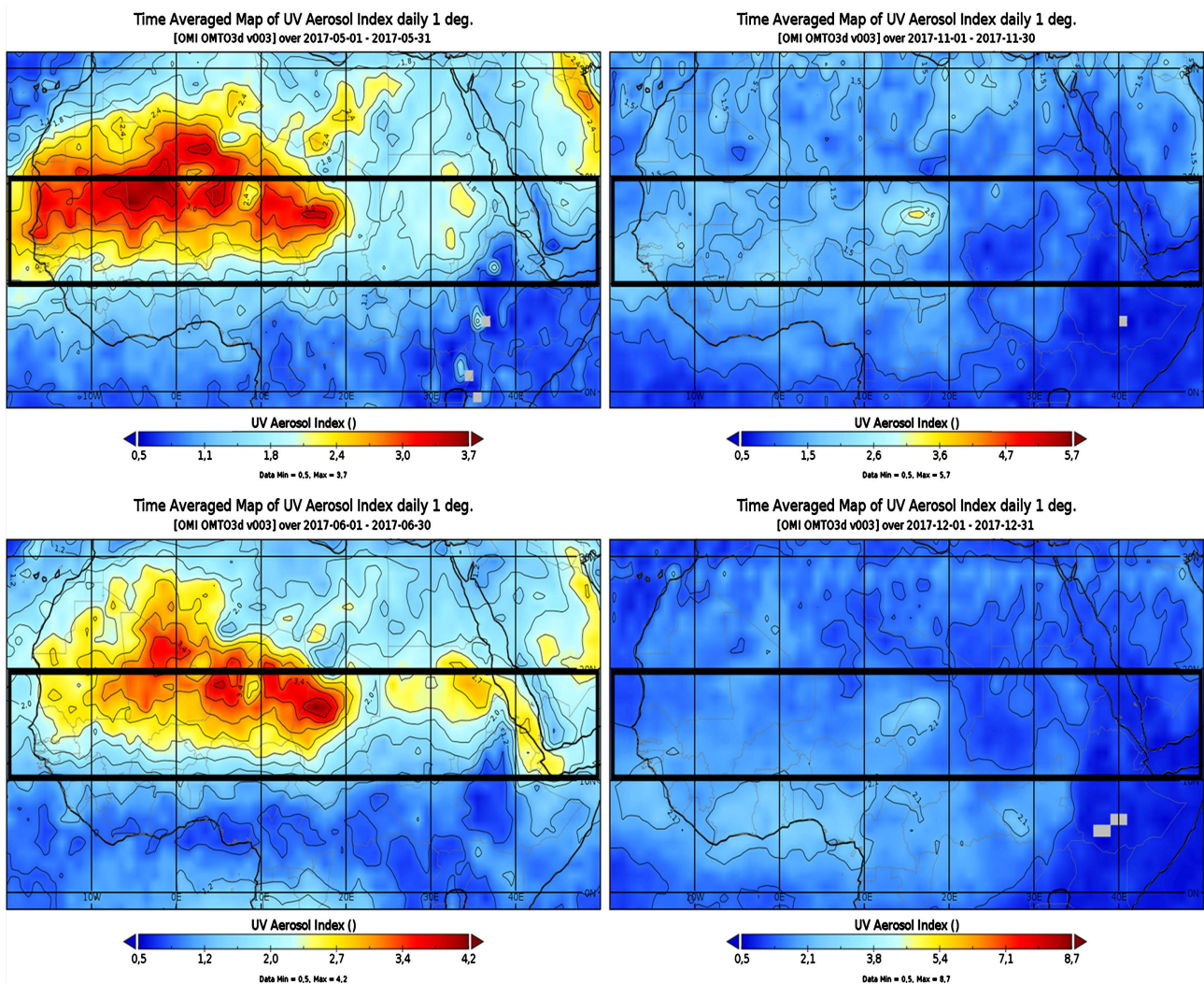


Figure 3. Observation of the UV Index aerosol distribution profile for OMI -2017 daily average with a resolution of 1.0×1.25 degrees. Data from the platform (from the Giovanni).

volcanic ash, biomass burning” from OMI and TOMS. These figures show a permanent presence of AUVI, in the 10 - 20 band over almost all the three measurement periods. It can also be seen that the “10.20°E” and “10.20°N” grids are almost always covered by AUVI, which can be explained by the fact that we are between Banizoumbou and the Bodélé depression. Two areas established as source areas for dust emissions (Bouet et al., 2012; Hudson-Edwards et al., 2014).

The study of the intra-annual variability of the AOD over Dakar and Banizoumbou for years with peaks greater than 2 gives:

Figure 4 and **Figure 5** which show the temporal variation of the Aerosol optical depth (AOD), the Angstrom coefficient and the precipitable water. In these two figures we note an intra-annual variation of the AOD, during the years for values higher than 2 for Dakar and 3 for Banizoumbou.

In **Figures 4(a)-(d)** peak values are observed. In 1997 there were three significant peaks where the OAD values reached 2, indicating a very high dust

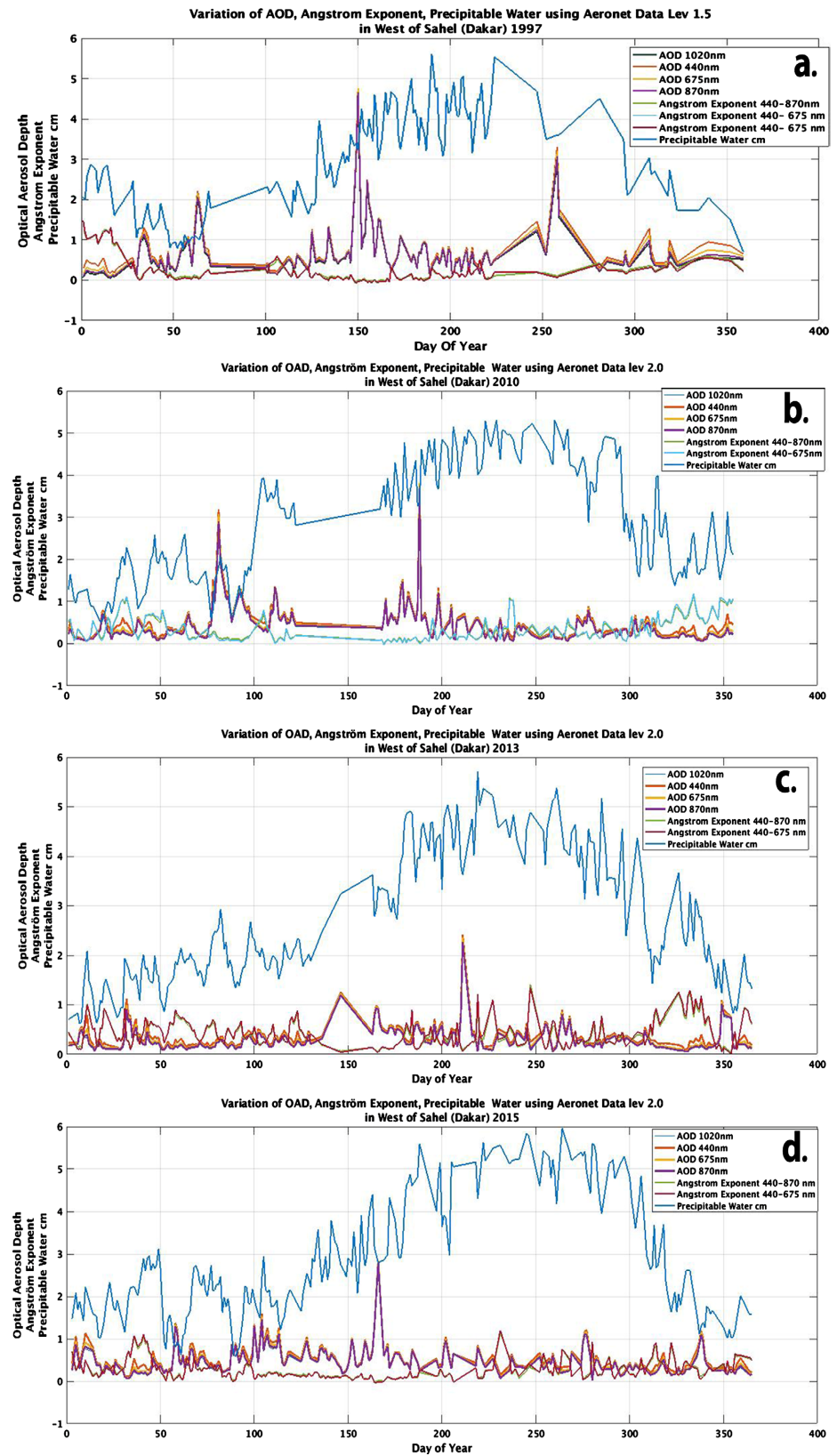


Figure 4. Intra-annual variation of the AOD, for years where the optical depth exceeded 2 from 1997 to 2018 in Dakar. (a) gives the variation of the AOD in 1997; (b) in 2010; (c) in 2013; (d) 2015 Aeronet.Nasa.Gouv data of level 1.5 for the station (Dakar).

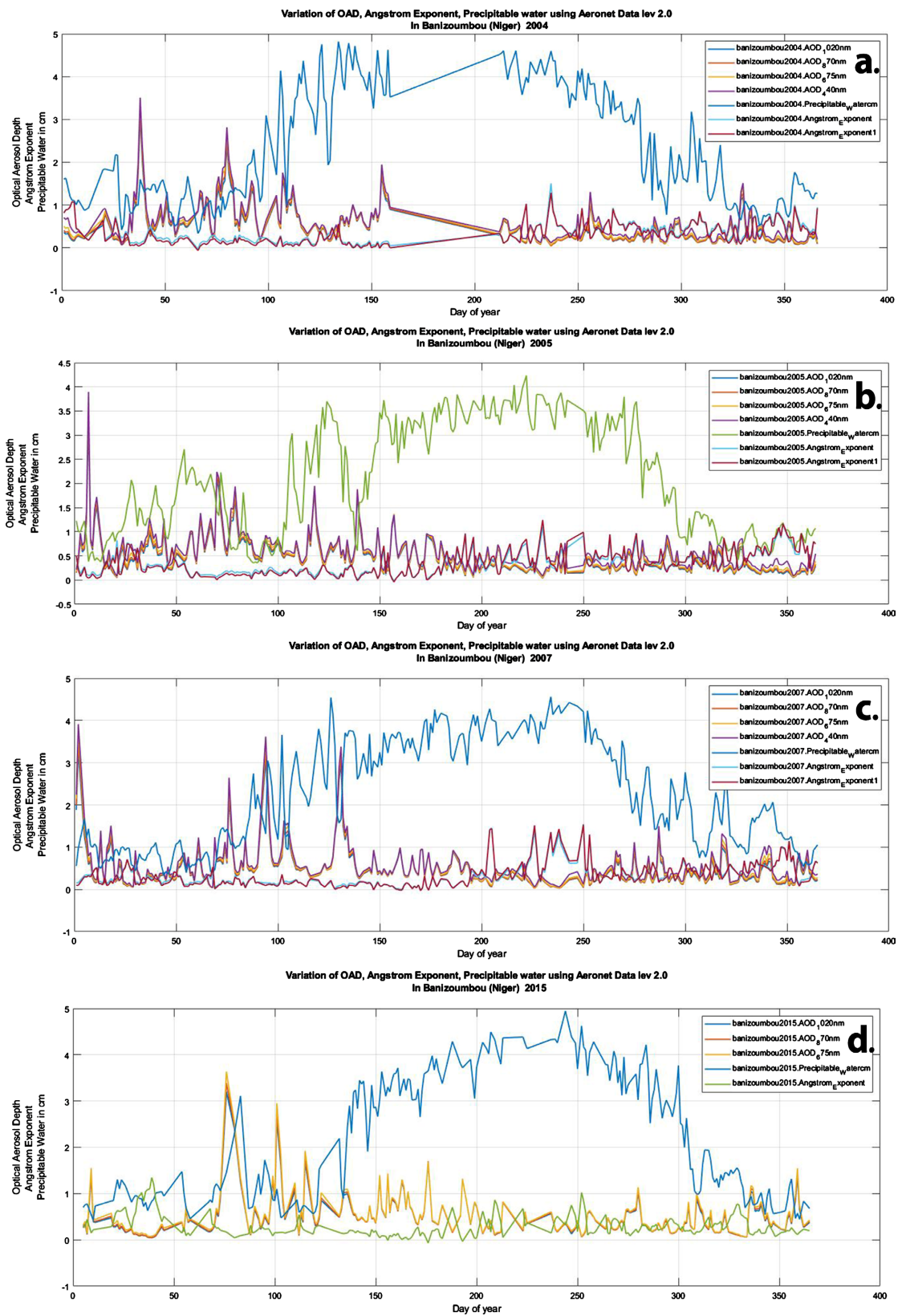


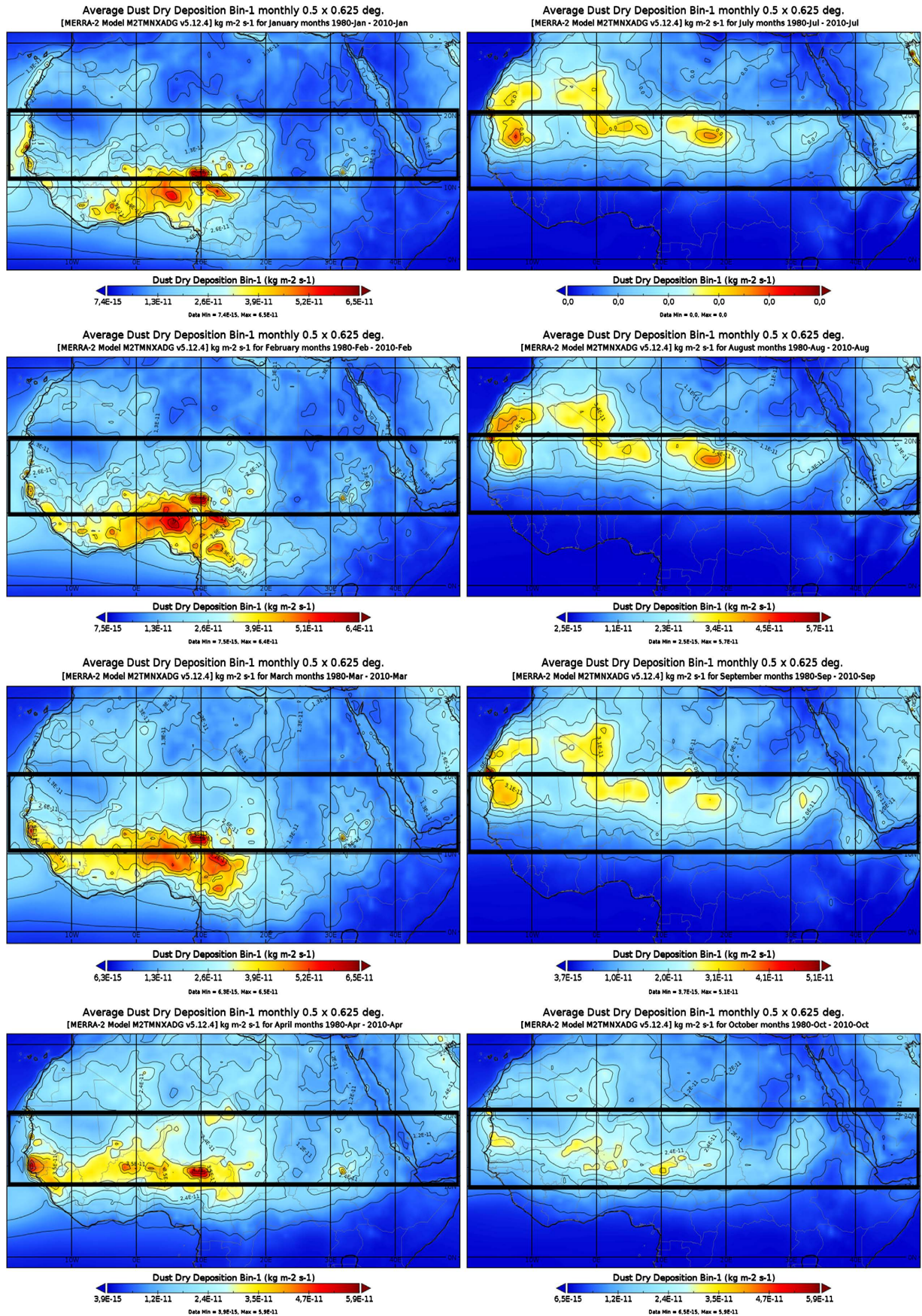
Figure 5. Intra-annual variation in AOD, for years where the optical depth exceeded 3 from 1997 to 2018. (a) gives the variation in AOD in 2004; (b) in 2005; (c) in 2007; (d) 2015 at Banizoumbou data from Aeronet.Nasa.Gouv (Banizoumbou).

presence with very low visibility in February, April and July. In 2010 there are two peaks in March and June. In 2013 and 2015 there is a peak in July for 2013 and in June for 2015. **Figures 5(a)-(d)** concern Banizoumbou; in 2004 peaks are noted in January, February and May. In 2005, there is a large peak in January, and smaller peaks in February and March. In 2007, peaks are noted in January, February, March and April. In 2015 the peaks are noted in February and March.

Overall, according to these in-situ data, the months of January and March in Banizoumbou are characterised by a very strong presence of dust with AODs reaching 3, which is a sign of a source area, or a location very close to a dust emission site. In Dakar, there is a time lag of about 10 to 25 days compared to the peak month in Banizoumbou, with an atmosphere that is just as dusty, but less so than in Banizoumbou. This allows us to assume that some of the Banizoumbou dust transits through the lower layers to Senegal.

At the time of and after the passage of the AUVIs, we note deposits in the 10 - 20 band. In fact, **Figure 6** shows that countries such as Senegal, the two Guineas, part of Mali, Burkina Faso, Niger, Chad and Nigeria are covered by deposition according to the month. These results can be found in some works for Mali ([McTainsh et al., 1997](#)) and Nigeria ([McTainsh, 1980](#)). From a climatic point of view, from 1980 to 2010, the presence of dust deposition in the 10 - 20 band is noted in all months. In January, the deposit spread from the 4th grid to the southwest. Thus the deposition starts from Chad with values around 2.6×10^{-11} Kg/m²/s and spreads over Niger with a strong accumulation in the South of Niger at the border with Nigeria of 6.5×10^{-11} Kg/m²/s. Deposits are also found on the Senegalese coast between 3.9×10^{-11} Kg/m²/s and 5.2×10^{-11} Kg/m²/s. This same profile is repeated in February; however, in March the deposition pattern between grid 1 (G1) and grid 2 (G2) becomes more and more zonal, with an increasingly important accumulation cluster in the southwest of Senegal. In April the maximum deposition profile becomes zonal with three marked spots in the North of Nigeria 4.7×10^{-11} Kg/m²/s, in the North of Burkina Faso 3.5×10^{-11} Kg/m²/s and at the Senegal-Guinea border 4.7×10^{-11} Kg/m²/s. In May the most important deposits are located in the South of Senegal. It can be seen that the deposition distribution has an increasingly latitudinal profile in the 10 - 20 band. It also rises towards the North. In June the deposition mainly covers the north of Senegal with a value of 4.4×10^{-11} Kg/m²/s; it also covers the north of Mali and part of Niger. In July, August, September the maximum deposition covers three large areas: Northern Senegal and South-West Mauritania; Northern Mali and Southern Algeria; The third is located between Niger and Chad. In October, November, December the deposit decreases in the 10 - 20 band and starts to form again towards Chad.

To find out whether a correlation exists between the different months with respect to deposition, a principal component analysis was performed. **Figure 7(a)** and **Figure 7(b)** show a scatterplot for individuals and the correlation circle for variables for the monthly dust deposition from 1980 to 2010.



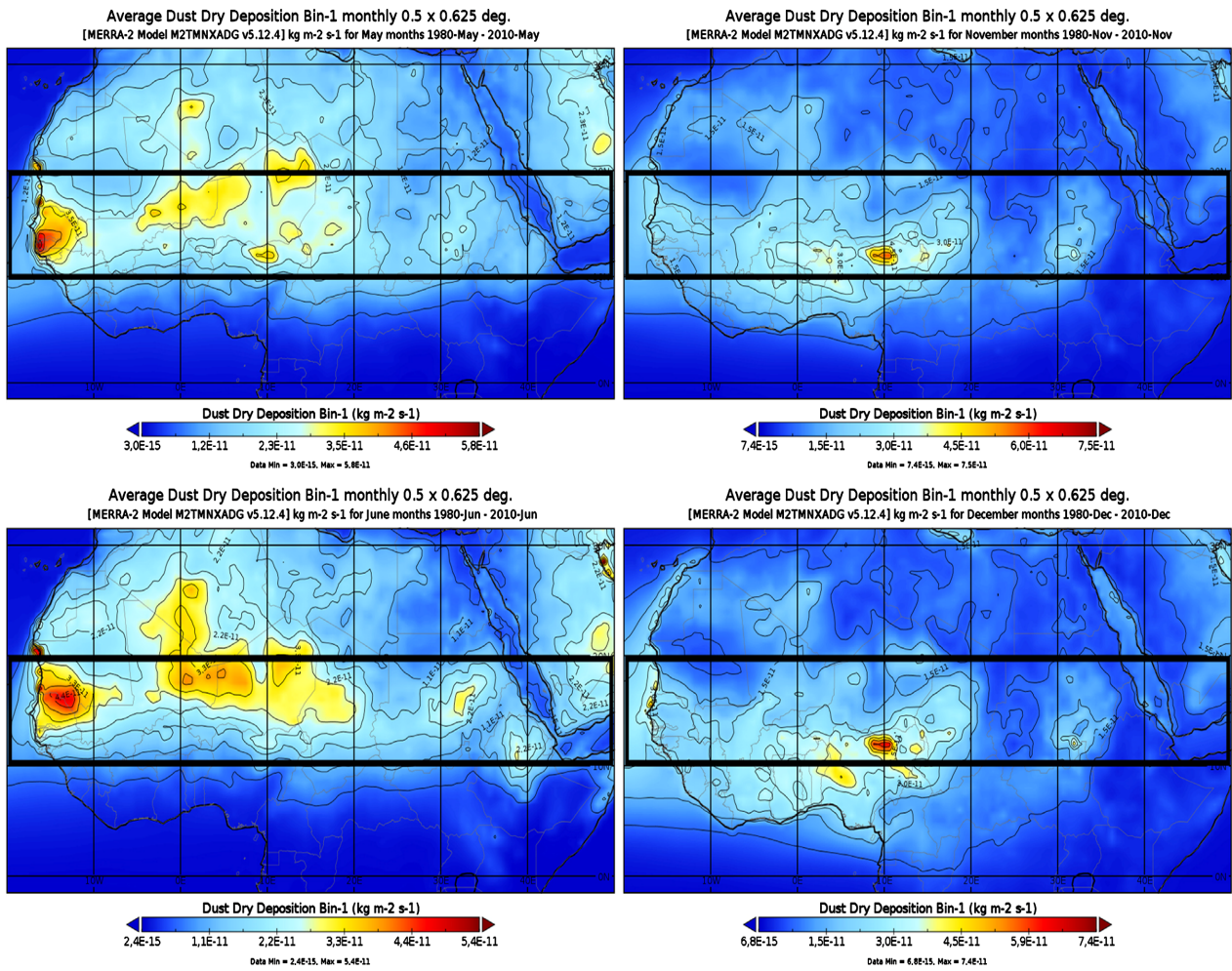


Figure 6. Climatology of monthly average dust deposition from 1980 to 2010 with [MERRA-2 Model M2TMNXADG v5.12.4] $\text{kg}\cdot\text{m}^{-2}\cdot\text{s}^{-1}$ data, for a resolution of $0.5 \times 0.5^\circ$. The black rectangle delimits the 10 - 20 African band.

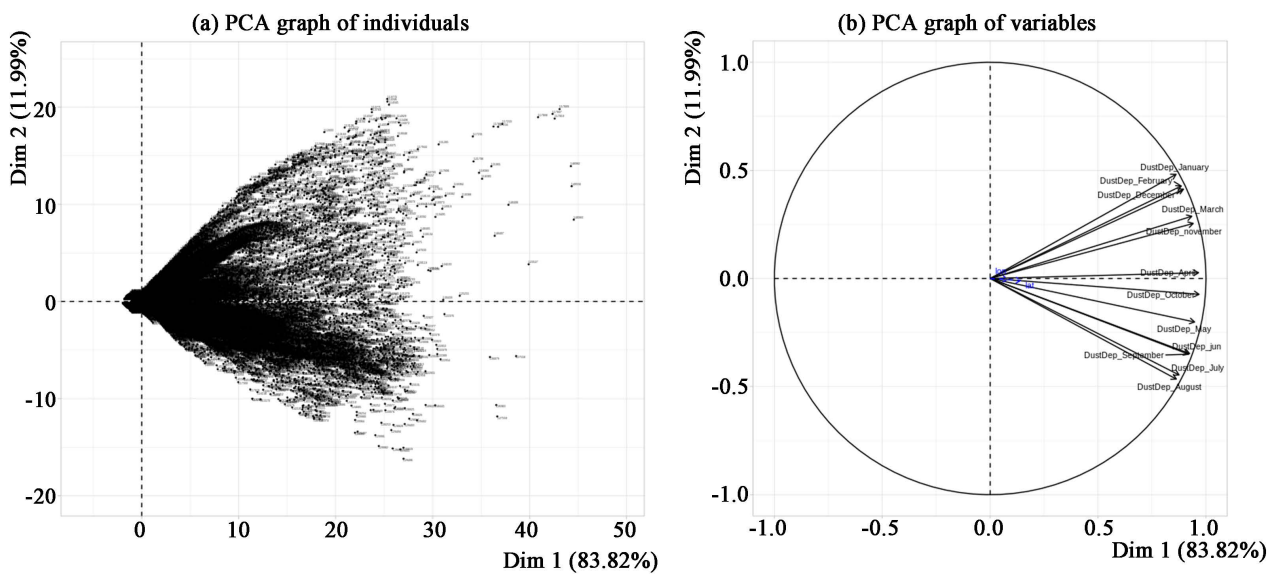


Figure 7. Principal component analysis of dust deposition climatology. (a) left: graph of individuals; (b) right: graph of variables, also called correlation circle.

All variables are located on either side of the first dimension which contains 83.82% of the information.

On dimension one, we have the April deposition so this dimension is well explained by this month.

Taking the maximum grids to restrict the clouds. We end up with **Figure 8** and **Figure 9**. We note that the 1st dimension is always well explained by the month of April.

Knowing that the eigenvalues can be used to determine the number of principal axes according to (Kaiser, 1961). In **Figure 10**, we have more than 70% of the information well explained by the first two dimensions of the PCA. The difference between the other remaining eigenvalues being relatively small, the first two axes explain well the relationships between the variables (Peres-Neto et al., 2005).

The red dotted line in **Figure 11** and **Figure 12** indicate the expected average contribution. If the contribution of the variables is uniform, the expected

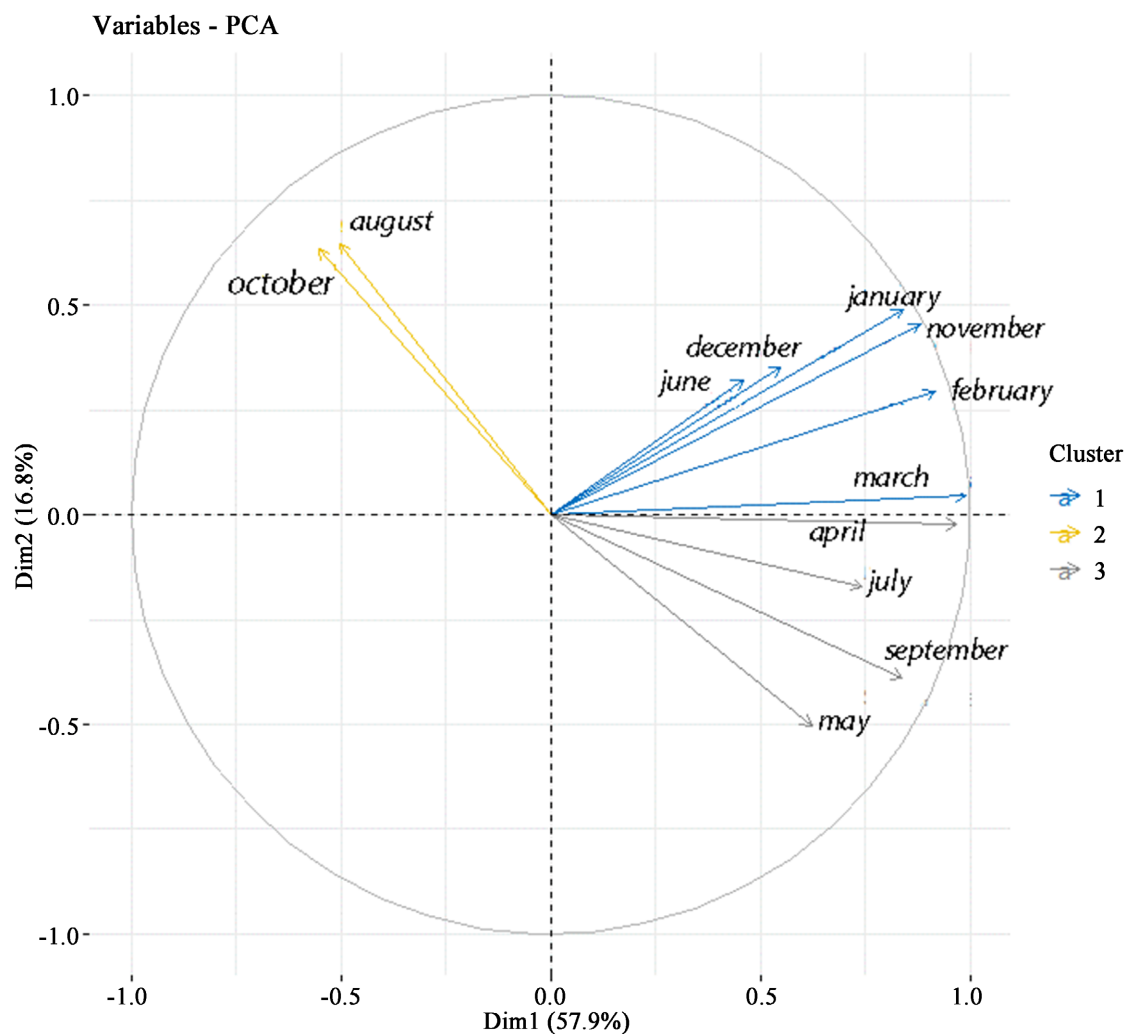


Figure 8. Principal component analysis of dust deposition climatology - graph of variables according to Maximum Grid (correlation circle).

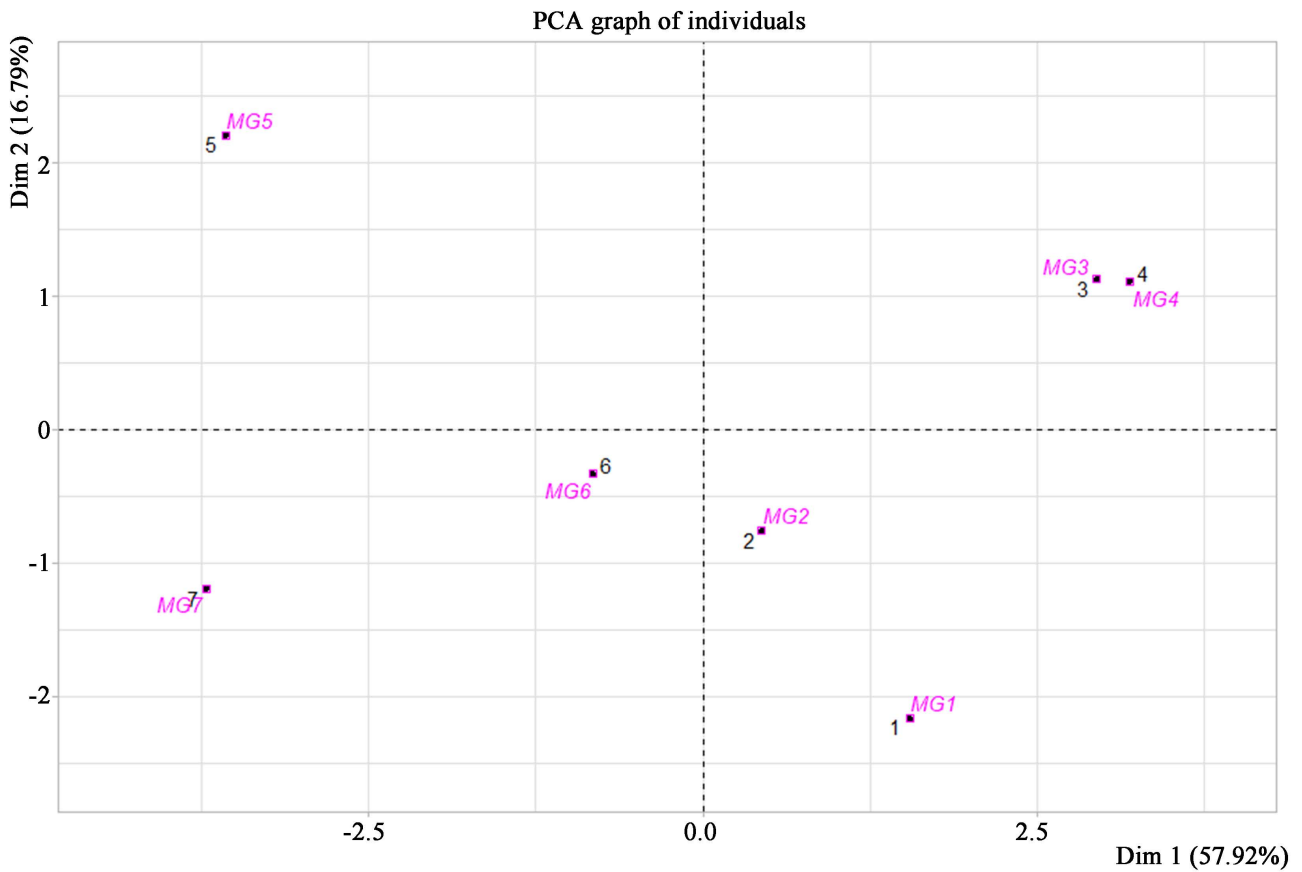


Figure 9. Principal component analysis of dust deposition climatology according to grid maximums (graph of individuals).

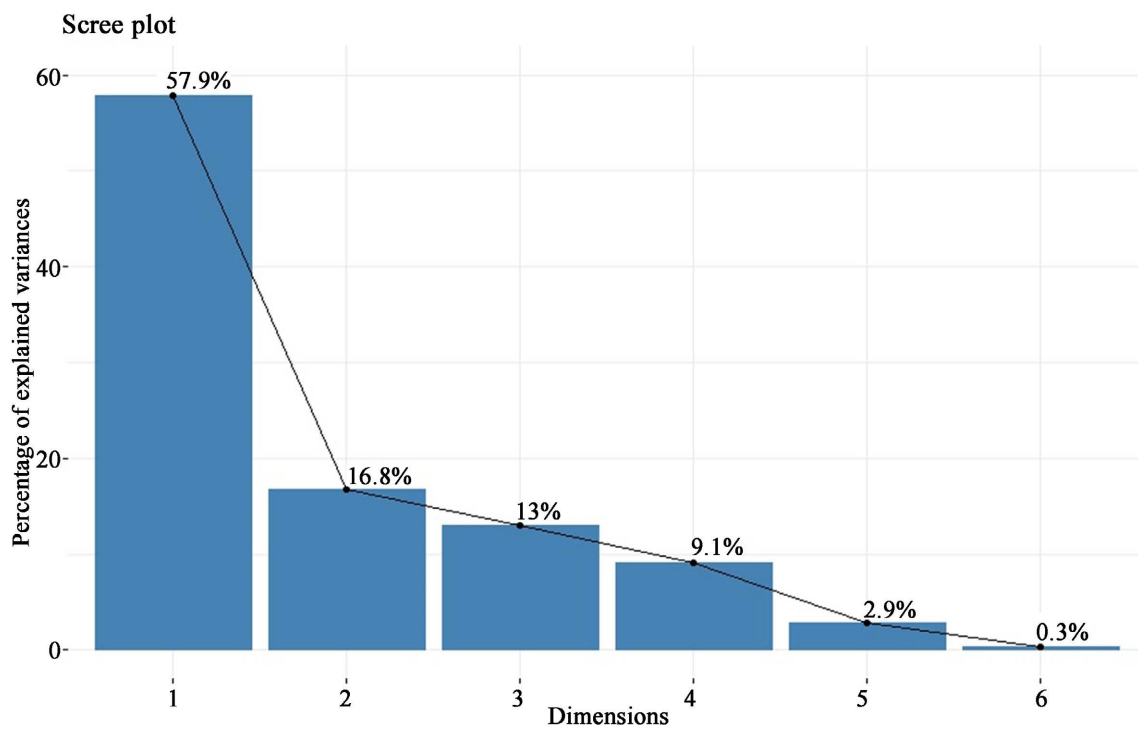


Figure 10. Eigenvalue plot for dust deposition against our PCA.

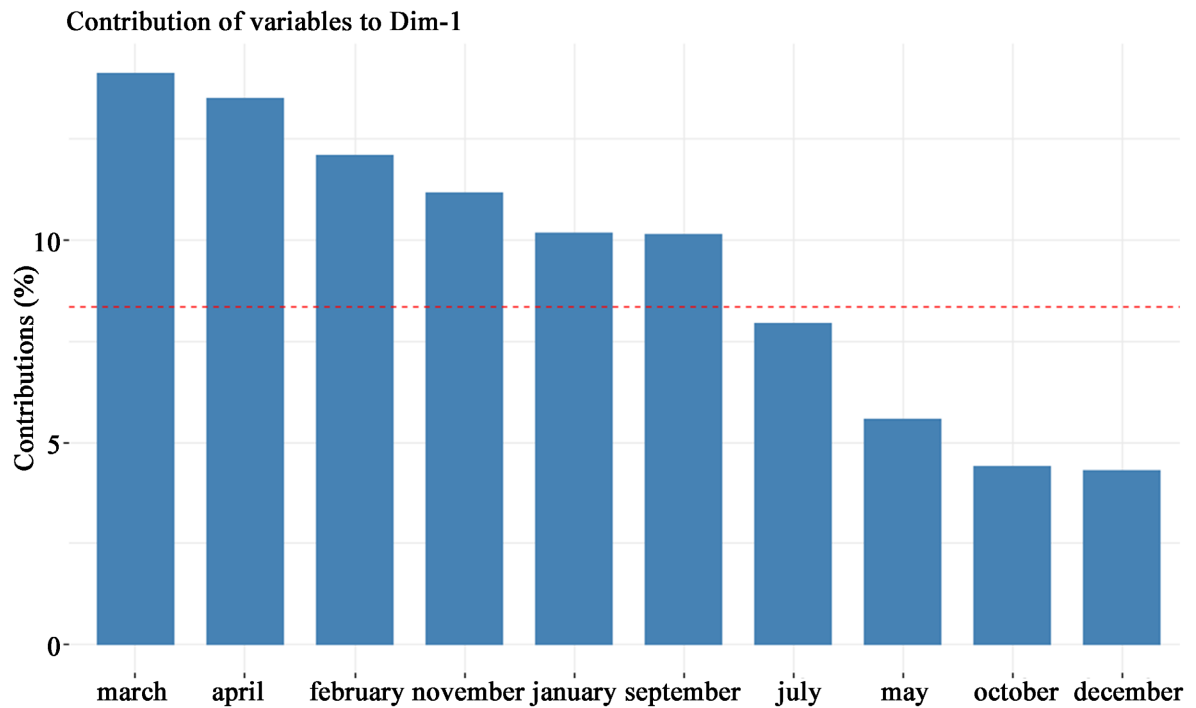


Figure 11. Graph of the contribution of the dust deposition variables to the first dimension of the PCA.

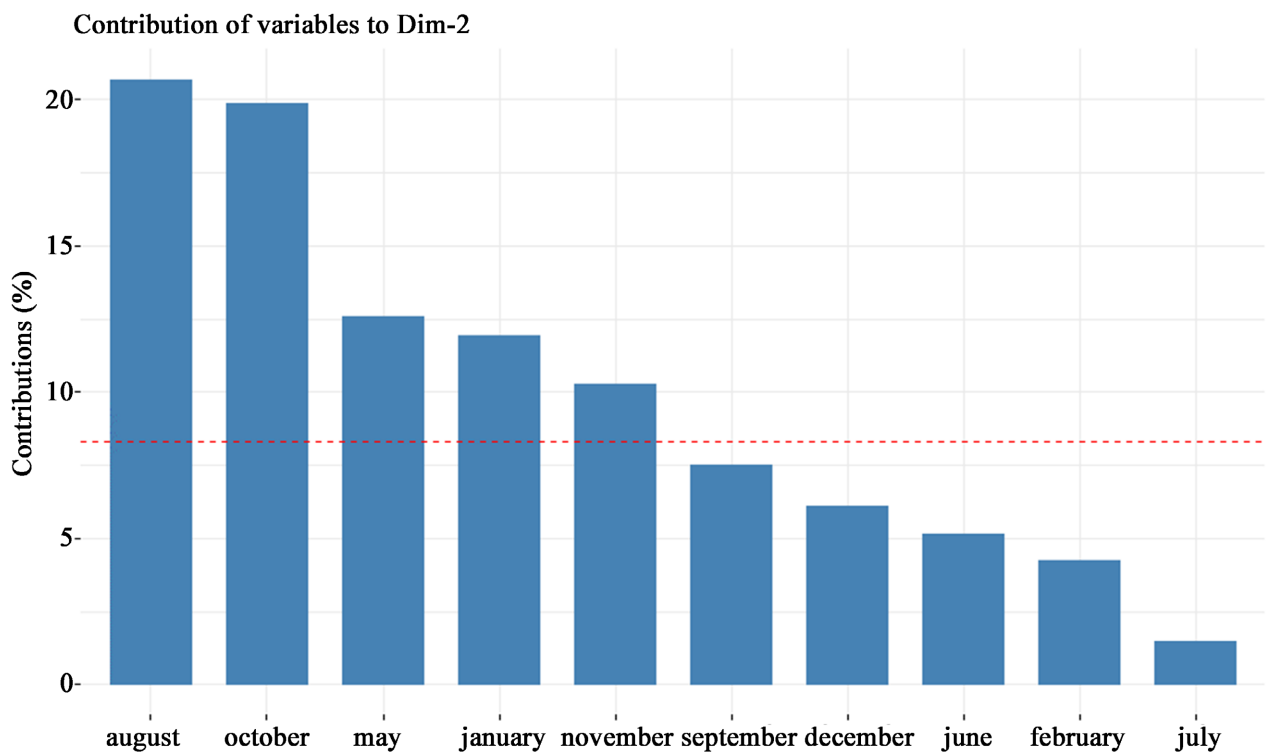


Figure 12. Graph of the contribution of the dust deposition variables to the second dimension of the PCA.

threshold value would be 10%. For a given component, a variable with a contribution above this threshold is considered to have a large contribution to the factorial axis. It can be seen that the deposit on each month except December con-

tributes well to the formation of the principal component analysis. This makes it possible to confirm the significance of the results given by the correlation circle.

Figure 13 shows a good contribution of the individuals that characterise the grids. **Figure 14** in turn summarises the good contribution of the variables to the 1st dimension of the PCA.

Figure 15 and **Figure 16** give us the graphs of the squared cosines associated with the variables in the PCA with respect to dimensions 1 - 2 and 2 - 3. A high \cos^2 indicates a good representation of the variable on the main axes under consideration. In this case, the variable is positioned near the circumference of the correlation circle. A low \cos^2 indicates that the variable is not perfectly represented by the main axes. In this case, the variable is close to the centre of the circle. For some of the variables, more than 2 axes may be needed to perfectly represent the data. In this case, the variables are positioned inside the correlation circle.

In summary: The \cos^2 values are used to estimate the quality of the representation. The closer a variable is to the correlation circle, the better its representation on the PCA map (and the more important it is for interpreting the principal components in consideration). Variables that are close to the centre of the chart are less important for the first components.

In our case, by associating **Figure 15** and **Figure 16**, we can say that we have a good quality of representation of the variables, which allows us to say that the results of the principal component analysis are significant.

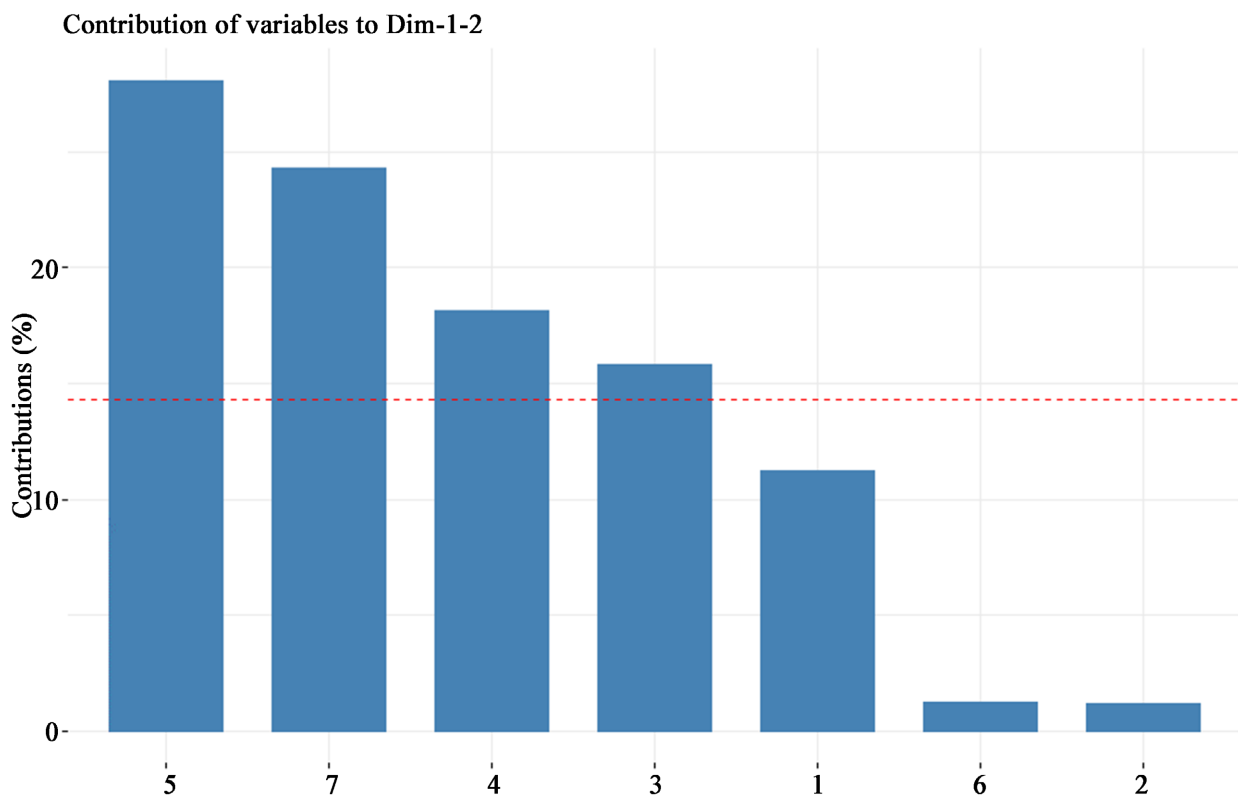


Figure 13. Graph of contribution of the individuals of the “dust deposition” compared to dimension 1-2 of the PCA.

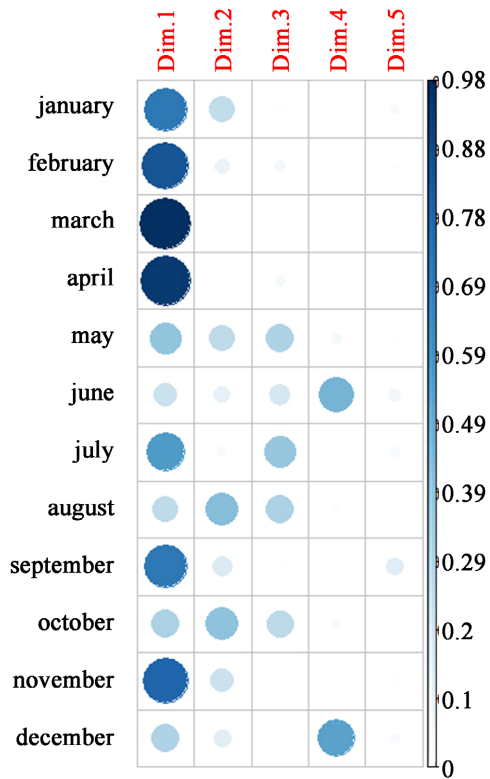


Figure 14. Graph of the contribution of dust deposition individuals to all dimensions of the PCA.

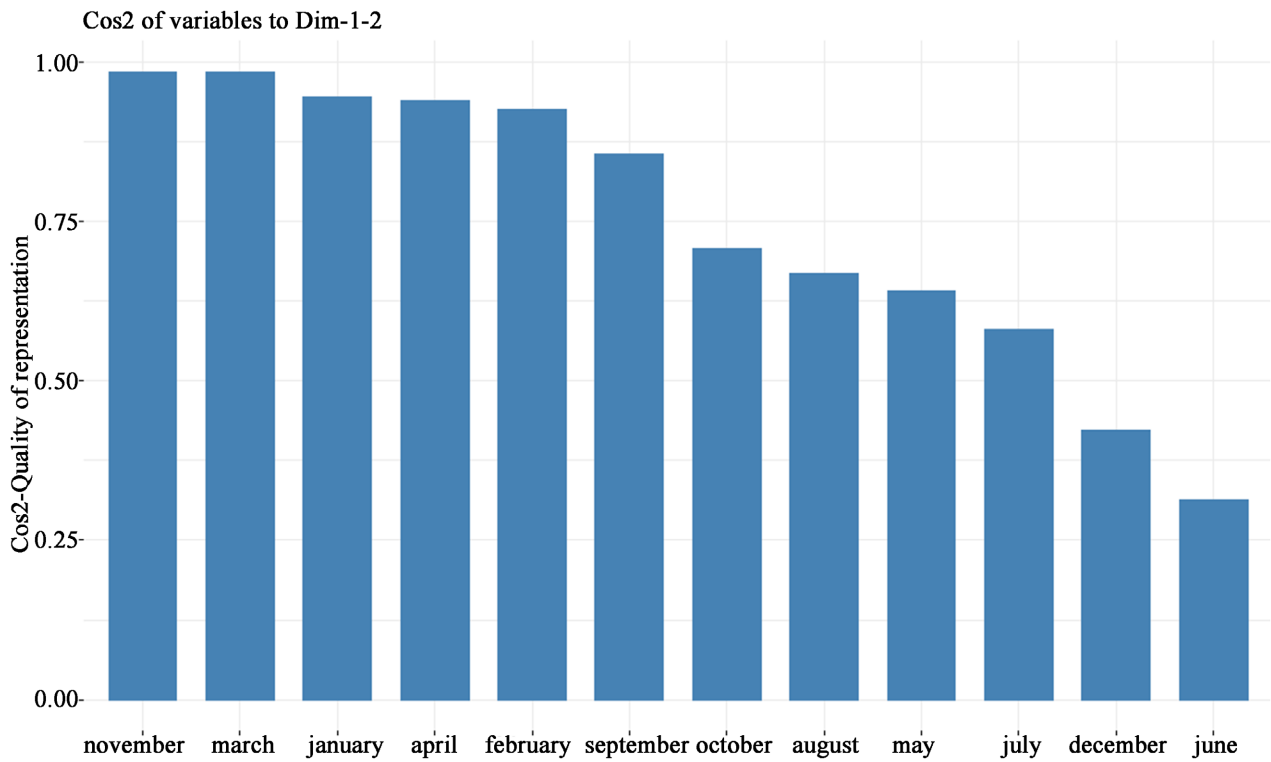


Figure 15. Quality graph of the representation of the dust deposition variables in relation to dimension 1-2 of the PCA.

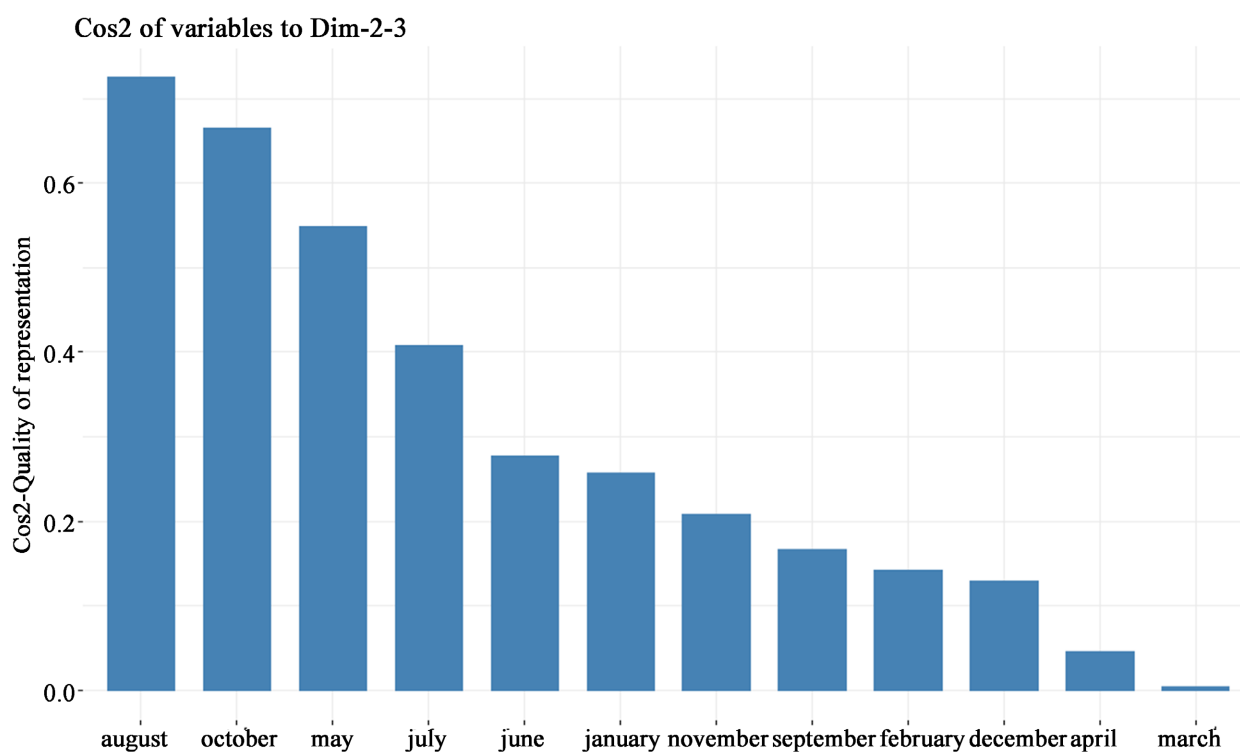


Figure 16. Quality graph of the representation of the dust deposition variables in relation to dimension 2-3 of the PCA.

The principal component analysis highlights a maximum of deposits in grids 3 and 4 in relation to the first factorial axis (dim1). This concerns Niger and part of Chad, which is explained by the fact that these two grids have been identified as source areas. According to the process of lifting, transport and deposition of fine particles, i.e. aerosols and the sandblasting process, most of the particles first fall on and around the same lifting area. For this reason, the maximum deposition occurs in the Niger and Chad area.

There is more or less significant deposition in grids 1 and 2. These two grids essentially cover Senegal and part of Mali. The PCA reveals a correlation between the deposition observed in the Chad-Niger region and the deposition in the Senegal-Malian region. After the lifting of aerosols in grids 3 and 4, particles smaller than or equal to 20 micrometres are transported over thousands of kilometres in the lower and middle layers of the atmosphere, and eventually arrive in grids 1 and 2. A time lag of about one and a half months is observed. A significant deposition is observed in January, February, June and August over the Chad-Niger region. As well as in the Senegal-Malian area in March, April, May, July and September.

Grids 5, 6 and 7 include Sudan, Eritrea, part of Ethiopia and Somalia. They are subject to very few deposits. The AUVI deposited in these areas is not correlated with what is happening in the rest of the 10 - 20 band.

4. Conclusion

Our study shows that over the three measurement periods, namely the TOMS

Nimbus-7 TOMSN7L3 v008 from 1978 to 1993, the TOMS EP TOMSEPL3 v008 from 1996-2005 and the OMI OMTO3d v003 from 2004 to 2008, the grid “10.20°E”, “10.20°N” is always covered by AUVI. This can be explained by the fact that we are between Banizoumbou and the Bodélé depression. The *in-situ* data show that Banizoumbou from January to March is characterised by a very high dust content. The AODs reach 3. For Dakar, a time lag of about 10 to 25 days is observed compared to the peak month of Banizoumbou. The atmosphere is just as dusty, but less so than at Banizoumbou. This allows us to assume that part of the Banizoumbou dust transits through the lower layers to Senegal. The statistical study shows a maximum of deposition in grids 3 and 4. This concerns Niger and part of Chad, which can be explained by the fact that these two grids have been identified as source areas. More or less significant deposition can be seen in grids 1 and 2. These two grids essentially cover Senegal and part of Mali. The PCA reveals a correlation between the deposition observed in the Chad-Niger region and the deposition in the Senegal-Malian region. A time lag of about 1.5 months is observed. A significant deposition is observed in January, February, June and August in the Chad-Niger region, as well as in the Senegal-Malian area in March, April, May, July and September.

The dust deposits in grids 5, 6 and 7 grouping Sudan, Eritrea, part of Ethiopia, and Somalia are not correlated with what is happening in the rest of the 10 - 20 band.

Acknowledgements

Our sincere thanks to CEA MITIC, UFRSAT and LMI ECLAIRS2 for supporting this work.

Conflicts of Interest

The authors declare no conflicts of interest regarding the publication of this paper.

References

- Abouchami, W., Nathe, K., Kumar, A., Galer, S. J., Jochum, K. P. et al. (2013). Geochemical and Isotopic Characterization of the Bodele Depression Dust Source and Implications for Transatlantic Dust Transport to the Amazon Basin. *Earth and Planetary Science Letters*, 380, 112-123. <https://doi.org/10.1016/j.epsl.2013.08.028>
- Acker, J. G., & Leptoukh, G. (2007). Online Analysis Enhances Use of NASA Earth Science Data. *Transactions American Geophysical Union*, 88, 14-17. <https://doi.org/10.1029/2007EO020003>
- Acker, J., Soebiyanto, R., Kiang, R., & Kempler, S. (2014). Use of the NASA Giovanni Data System for Geospatial Public Health Research: Example of Weather-Influenza Connection. *International Journal of Geo-Information*, 3, 1372-1386. <https://doi.org/10.3390/ijgi3041372>
- Adenira, F. O., Musa, S. Y., & Johnson, A. O. (2019). Statistical Modelling of Atmospheric Mean Temperature in Sub-Sahel West Africa. *Scientific African*.
- Ali, A. (2008). Meaning and Use of the Rainfall Index in the Sahel. *Science and Planetary*

Change/Drought, 19, 227-235.

- Alimen, H. (1897). Evolution of the Climate and Civilizations for 40,000 Years from North to South of Western Sahara (First Conceptions Confronted with Current Data). *Quaternaire*, 215-227.
- Apoil, P. A., & Yacouba, T. (2018). Particular Aspects of Allergies in Sahelian Africa. *French Journal of Allergology*, 58, 23-28. <https://doi.org/10.1016/j.reval.2017.07.009>
- Basar, S., Perez, C., Cuevas, E., Baldasano, J. M., & Gobbi, G. P. (2009). Aerosol Characterization in Northern Africa, Northeastern Atlantic, Mediterranean Basin and Middle East from Direct-Sun AERONET Observations. *Atmospheric Chemistry and Physics*, 9, 8265-8282. <https://doi.org/10.5194/acp-9-8265-2009>
- Bouet, C., Cautenet, G., Bergametti, G., Marticorena, B., Todd, M. C., & Washington, R. (2012). Sensitivity of Desert Dust Emissions to Model Horizontal Grid Spacing during the Bodélé Dust Experiment 2005. *Atmospheric Environment*, 50, 377-380. <https://doi.org/10.1016/j.atmosenv.2011.12.037>
- Buontempo, C., Scientist, S., & Centre, M. O. (2010). *Climat Sahélien: Rétrospective et Projections*. Issy-les-Moulineaux: Met Office.
- Dirk, S., Schütz, L., Kandler, K., Ebert, M., & Weinbruch, S. (2013). Bulk Composition of Northern African Dust and Its Source Sediments—A Compilation. *Earth-Science Reviews*, 116, 170-194. <https://doi.org/10.1016/j.earscirev.2012.08.005>
- Durand, A., & Lang, J. (1991). Breaks in the Continental Environmental Equilibrium and Intensity Changes in Aridity over the Past 20 000 Years in the Central Sahel. *Journal of African Earth Sciences*, 12, 199-208. [https://doi.org/10.1016/0899-5362\(91\)90069-B](https://doi.org/10.1016/0899-5362(91)90069-B)
- Goodman, M. M., Carling, G. T., Fernandez, D. P., Rey, K. A., Hale, C. A., Bickmore, B. R., Nelson, S. T., & Munroe, J. S. (2019). Trace Element Chemistry of Atmospheric Deposition along the Wasatch Front (Utah, USA) Reflects Regional Playa Dust and Local Urban Aerosols. *Chemical Geology*, 530, 119317. <https://doi.org/10.1016/j.chemgeo.2019.119317>
- Hassane, B., Durand, A., Gar, Z., Dieppois, B., Sebag, D., Rajot, J. L., & Traore, A. (2016). Can Daily Meteorological Measurement of Near-Surface Wind Detect Climate Changes in the Sahel (SE Niger, 1950-1992)? *Journal of Arid Environments*, 124, 91-101. <https://doi.org/10.1016/j.jaridenv.2015.07.014>
- Hooker, S. B., & McClain, C. R. (2000). The Calibration and Validation of SeaWiFS Data. *Progress in Oceanography*, 45, 427-465. [https://doi.org/10.1016/S0079-6611\(00\)00012-4](https://doi.org/10.1016/S0079-6611(00)00012-4)
- Huber, S., & Fensholt, R. (2011). Analysis of Teleconnections between AVHRR-Based Sea Surface Temperature and Vegetation Productivity in the Semi-Arid Sahel. *Remote Sensing of Environment*, 115, 3276-3285. <https://doi.org/10.1016/j.rse.2011.07.011>
- Hudson-Edwards, K. A., Bristow, C. S., Cibin, G., Mason, G., & Peacock, C. L. (2014). Solid-Phase Phosphorus Speciation in Saharan Bodélé Depression Dusts and Source Sediments. *Chemical Geology*, 384, 16-26. <https://doi.org/10.1016/j.chemgeo.2014.06.014>
- Janicot, S. (2009). A Comparison of Indian and African Monsoon Variability at Different Time Scales. *Comptes Rendus Geoscience*, 341, 575-590. <https://doi.org/10.1016/j.crte.2009.02.002>
- Kahn, R. A., Gaitley, B. J., Martonchik, J. V., Diner, D. J., & Crean, K. A. (2005). Multian-gle Imaging Spectroradiometer (MISR) Global Aerosol Optical Depth Validation Based on 2 Years of Coincident Aerosol Robotic Network (AERONET) Observations. *Journal of Geophysical Research: Atmospheres*, 110, D10S04. <https://doi.org/10.1029/2004JD004706>

- Kaiser, H. F. (1961). A Note on Guttman's Lower Bound for the Number of Common Factors. *British Journal of Statistical Psychology*, 14, 1-2. <https://doi.org/10.1111/j.2044-8317.1961.tb00061.x>
- Lavaysse, C., Flamant, C., Janicot, S., Parker, D. J., Lafore, J. P., Sultan, B., & Pelon, J. (2009). Seasonal Evolution of the West African Heat Low: A Climatological Perspective. *Climate Dynamics*, 33, 313-330. <https://doi.org/10.1007/s00382-009-0553-4>
- Lebel, T., & Vischel, T. (2005). Climat et cycle de l'eau en zone tropicale: Un problème d'échelle. *Comptes Rendus Geoscience*, 337, 29-38. <https://doi.org/10.1016/j.crte.2004.08.011>
- Lézine, A. M., Hély, C., Grenier, C., Braconnot, P., & Krinner, G. (2011). Sahara and Sahel Vulnerability to Climate Changes, Lessons from Holocene Hydrological Data. *Quaternary Science*, 30, 3001-3012. <https://doi.org/10.1016/j.quascirev.2011.07.006>
- Li, R., Ma, X., Xiong, F., Jia, H., Sha, T., & Tian, R. (2020). Comparisons and Evaluation of Aerosol Burden and Optical Depth in CMIP5 Simulations over East Asia. *Journal of Atmospheric and Solar-Terrestrial Physics*, 206, 105315. <https://doi.org/10.1016/j.jastp.2020.105315>
- Marticorena, B., & Bergametti, G. (1995). Modeling the Atmospheric Dust Cycle. Part 1: Design of a Soil-Derived Dust Emission Scheme. *Journal of Geophysical Research Atmospheres*, 100, 16415-16430. <https://doi.org/10.1029/95JD00690>
- McTainsh, G. (1980). Harmattan Dust Deposition in Northern Nigeria. *Nature*, 286, 587-588. <https://doi.org/10.1038/286587a0>
- McTainsh, G. H., Nickling, W. G., & Lynch, A. W. (1997). Dust Deposition and Particle Size in Mali, West Africa. *CATENA*, 29, 307-322. [https://doi.org/10.1016/S0341-8162\(96\)00075-6](https://doi.org/10.1016/S0341-8162(96)00075-6)
- Memiche, M., Bouzian, C., Benzahia, A., & Moussi, A. (2020). Effects of Dust, Soiling, Aging, and Weather Conditions on Photovoltaic System Performances in a Saharan Environment—Case study in Algeria. *Global Energy Interconnection*, 3, 60-67. <https://doi.org/10.1016/j.gloi.2020.03.004>
- Olauson, J. (2018). ERA5: The New Champion of Wind Power Modelling? *Renewable Energy*, 126, 322-331. <https://doi.org/10.1016/j.renene.2018.03.056>
- Peres-Neto, P. R., Jackson, D. A., & Somers, K. M. (2005). How Many Principal Components? Stopping Rules for Determining the Number of Non-Trivial Axes Revisited. *British Journal of Statistical Psychology*, 49, 974-997. <https://doi.org/10.1016/j.cpsda.2004.06.015>
- Rajot, J. L., Toure, A., Guillon, R., Zibogarba Petit, C., Bichet, V., & Marticorena, B. (2011). Les poussières terrigènes au Sahel—Un marqueur climatique ou anthropique? *Colloque International: Sciences de l'Eau, du Climat et de l'Environnement pour un Développement Durable de l'Afrique, Ngaoundéré (CMR)*, 50.
- Redelsperger, J. L., Diedhiou, A., Flamant, C., Janicot, S., Lafore, J. P., Lebel, T., & Marticorena, B. (2006). Amma, une étude multidisciplinaire de la mousson ouest-africaine. *La Météorologie*, 54, 22-32. <https://doi.org/10.4267/2042/20098>
- Si, Y., Chen, L., Xiong, X., Shi, S., Husi, L., & Cai, K. (2019). Evaluation of the MISR Fine Resolution Aerosol Product Using MODIS, MISR, and Ground Observations over China. *Atmospheric Environment*, 223, 117229. <https://doi.org/10.1016/j.atmosenv.2019.117229>
- Tassan, S. (1994). Local Algorithms Using SeaWiFS Data for the Retrieval of Phytoplankton, Pigments, Suspended Sediment, and Yellow Substance in Coastal Waters. *Applied Optics*, 33, 2369-2378. <https://doi.org/10.1364/AO.33.002369>
- Touré, A. A., Tidjani, A., Rajot, J., Marticorena, B., Bergametti, G., Bouet, C., Ambouta,

- K. J. M., & Garba, Z. (2019). Dynamics of Wind Erosion and Impact of Vegetation Cover and Land Use in the Sahel: A Case Study on Sandy Dunes in Southeastern Niger. *Catena*, *177*, 272-285. <https://doi.org/10.1016/j.catena.2019.02.011>
- Wang, C., Graham, R. M., Wang, K., Gerland, S., & Granskog, M. A. (2019). Comparison of ERA5 and ERA-Interim Near-Surface Air Temperature, Snowfall and Precipitation over Arctic Sea Ice: Effects on Sea Ice Thermodynamics and Evolution. *The Cryosphere*, *13*, 1661-1679. <https://doi.org/10.5194/tc-13-1661-2019>